International Journal of Heat and Mass Transfer 182 (2022) 121962

Contents lists available at ScienceDirect

International Journal of Heat and Mass Transfer

journal homepage: www.elsevier.com/locate/hmt

On the thermocapillary migration between parallel plates

Qingwen Dai[a,b,*], Sangqiu Chen[a], Wei Huang[a], Xiaolei Wang[a], Steffen Hardt[b]

[a] National Key Laboratory of Science and Technology on Helicopter Transmission, Nanjing University of Aeronautics & Astronautics, Nanjing 210016, China
[b] Institute for Nano- and Microfluidics, Technische Universitat Darmstadt, Darmstadt 64287, Germany

ARTICLE INFO

Article history:
Received 18 June 2021
Revised 18 August 2021
Accepted 10 September 2021

Keywords:
Thermocapillary migration
Hele-Shaw cell
Liquid bridge
Air bubble

ABSTRACT

In this work, the thermocapillary migration of liquid bridges and air bubbles between parallel plates is studied. The factors influencing the thermocapillary migration are discussed, especially the magnitudes of the thermal gradient, the liquid or gas volume and the tilt angle of the parallel plates against gravity. The experimental trends are explained based on scaling models. It is found that a critical tilt angle exists at which the thermocapillary migration of liquid bridges is suspended. A simple two-dimensional theoretical model for the migration of liquid bridges is formulated. The model is able to predict the critical tilt angles in an approximate manner. An application perspective of this work lies in tribological systems in which liquid lubricant is replenished using applied thermal gradients.

1. Introduction

Thermocapillary migration is a phenomenon caused by the Marangoni effect in which a flow is created along an interface between two fluids due to interfacial tension gradient [1–6]. Since the liquid/gas interfacial tension decreases with increasing temperature, a thermal gradient leads to an interfacial tension gradient, actuating a locomotion from low to high tension regions. One can utilize this thermal effect in different contexts, for example to modify the wettability of surfaces [7], to improve heat exchange efficiency [8], or to induce directional transport [9]. In some specific applications, for example, frictional heat at surfaces gliding past each other can yield an unexpected migration of liquid lubricants, resulting in boundary lubrication [10].

Over the past years, extensive research has been conducted on the thermocapillary migration of liquid droplets [11–16]. Theoretical models describing this phenomenon were originally proposed by Greenspan [17], and further elaborated by Brochard [18], Ford et al. [19] as well as Pratap et al. [20]. These models are based on balancing the thermocapillary driving force and the internal viscous resistance force acting on the droplet. Taking into account the temperature dependence of viscosity [21], contact angle hysteresis [22], or contact line dynamics [23] improves the accuracy of models. Experimentally, decorating solid surfaces with micro/nano structures [24-28] or chemical coatings [29], designing new lubricants [30], applying external electrical fields [31] or mechanical vibration [32] provide help in controlling the droplet motion. These contributions have provided clear insights into the physical effects and control schemes related to the thermocapillary migration of liquid on free solid surfaces.

Here, free solid surfaces are referred to as solid surfaces delimiting a virtually infinitely extended domain. In reality, however, thermocapillary migration often occurs between two solid surfaces. Then, the sessile droplets on free solid surfaces transform into liquid bridges. For droplets, interfacial forces just act in the vicinity of the three-phase contact line on one solid surface, while for liquid bridges, significant forces exist at both the lower and upper surface. Recently, we preliminarily studied the migration of liquid bridges between a sphere and a plate, casting a glimpse on the migration phenomena at the interface [33]. Nevertheless, the fundamental understanding of the thermocapillary motion of liquid bridges, as well as the related influencing factors and fluid dynamic phenomena remains limited.

In fact, not only small-scale liquid bridges, but also larger-scale ones exist between two solid surfaces. Moreover, air bubbles can easily nucleate in the liquid between two solid surfaces, which means that migration phenomena of liquid bridges and air bubbles between two surfaces can even occur simultaneously. Besides, parallel plates are not always arranged horizontally in the mechanical system, which means that gravity acts as an additional driving force. All of the above-mentioned phenomena need to be understood to guide the design of advanced lubrication systems.

Hence, in this work, the thermocapillary migration of liquid bridges and air bubbles between parallel plates, i.e. in a Hele-Shaw cell, is studied. Special attention is paid to the migration behavior between tilted parallel plates, and critical tilt angles corresponding to elimination of thermocapillary migration are investigated. A

* Corresponding author at: National Key Laboratory of Science and Technology on Helicopter Transmission, Nanjing University of Aeronautics & Astronautics, Nanjing 210016, China.
E-mail address: daiqingwen@nuaa.edu.cn (Q. Dai).

https://doi.org/10.1016/j.ijheatmasstransfer.2021.121962
0017-9310/

theoretical model is established to predict the thermocapillary migration and the critical tilt angle. *In situ* observation of thermally driven flow is conducted to figure out the internal mechanism.

2. Materials and methods

2.1. Materials

Silicone oils are commonly used as lubricants, among others because they remain stable at comparatively high temperatures. Here, a typical type of silicone oil with a viscosity of 100 mPa·s, as received from a commercial supplier, was utilized in all experiments (purity > 95%, Sinopec Yangzi Petrochemical Company, China). Its physical properties are listed in Table 1. The surface tension of silicone oil was measured via the Wilhelmy plate method, and the temperature derivative of surface tension was calculated based on surface-tension values at different temperatures (the measured data are provided in Fig. S1). Apparent contact angles of silicone oil on the stainless steel and quartz glass surfaces were measured via the sessile drop method.

2.2. Methods

Fig. 1a shows the schematic of the experimental apparatus designed for this study. The parallel plates are arranged on a tiltable platform. For the sake of observation, the upper plate is made of quartz glass, and the dimensions of the testing region are 90 × 14 × 0.25 mm (length × width × height) with an average surface roughness of ~5 nm. The lower plate is made of stainless steel 316 with dimensions of 90 × 14 × 1.5 mm (length × width × height) and an average surface roughness of ~50 nm. The gap between the upper and lower plate was fixed to a constant value of 1.25 mm via two copper blocks.

Table 1
Physical properties of the used silicone oil at 298 K.

Parameter	Symbol	Value
Dynamic viscosity	μ	100±5 mPa/s
Density	ρ	963 kg/m^3
Surface tension	γ	21±0.1 mN/m
Temperature derivative of surface tension	γ_T	0.046±0.002 mN/(m K)
Thermal diffusivity	k	~0.15 mm^2/s
Contact angle on stainless steel	θ_{steel}	10±0.5°
Contact angle on quartz glass	θ_{glass}	13±0.5°

Table 2
Experimental conditions.

Interface gap	1.25 mm
Ambient temperature	298 K
Thermal gradient	3, 4.3, 5, 5.9 K/mm
Liquid volume	20, 40 and 400 μL
Tilt angle	1.2, 2.2, 2.4, 2.6, 2.8, 3.2°

Two ends of the lower plate were fixed on temperature-controllable heating and cooling elements to generate a thermal gradient along the solid surface. Two type-K thermocouples (accuracy of ± 1.5 K), fixed right under the two ends of the lower plate, were used to measure the temperature. The lower plate was embedded in a ceramic chamber to avoid heat loss and leakage of lubricants. After the imposed thermal gradient had stabilized, silicone oil droplets were injected between the surfaces via a microsyringe (diameter of needle: 0.4 mm, at room temperature) within a short period of approximately 1 s. The migration processes of liquid bridges from bird's eye and side views were captured via a digital camera (Nikon D750, Japan) and a digital microscope (Keyence VHX-600, Japan).

Fig. 1b shows a typical migration phenomenon of a liquid bridge subjected to a thermal gradient of 3 K/mm. The two plates were arranged horizontally and the volume of silicone oil was 20 μL. Under the effect of a thermal gradient, the liquid bridge migrates from the hot to the cold side (bird's eye view), and the geometrical shape of liquid bridge could be recorded from the side view. The main experimental parameters are listed in Table 2.

3. Results and discussion

3.1. Migration of liquid bridges between horizontal parallel plates

Fig. 2a shows the migration phenomenon of liquid bridges with volumes of 20 and 40 μL between horizontal parallel plates. Different thermal gradients of 3.0, 4.3 and 5.9 K/mm were tested and frames of the dynamic process within a migration distance of ~16 mm were recorded, as shown in Fig. 2a. Detailed migration process of the 40 μL liquid bridge can be seen in the Video S1 (in Supplementary material). Taking the advancing edge of a liquid bridge as a reference, the migration distance was measured and is shown in Fig. 2b as a function of time.

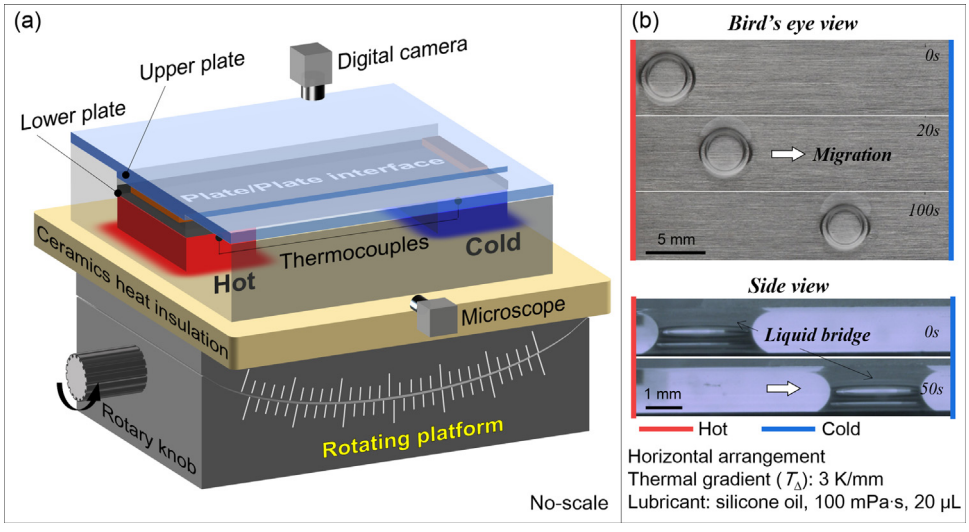

Fig. 1. (a) Schematic of the experimental apparatus, (b) bird's eye and side views of the migration process of a liquid bridge.

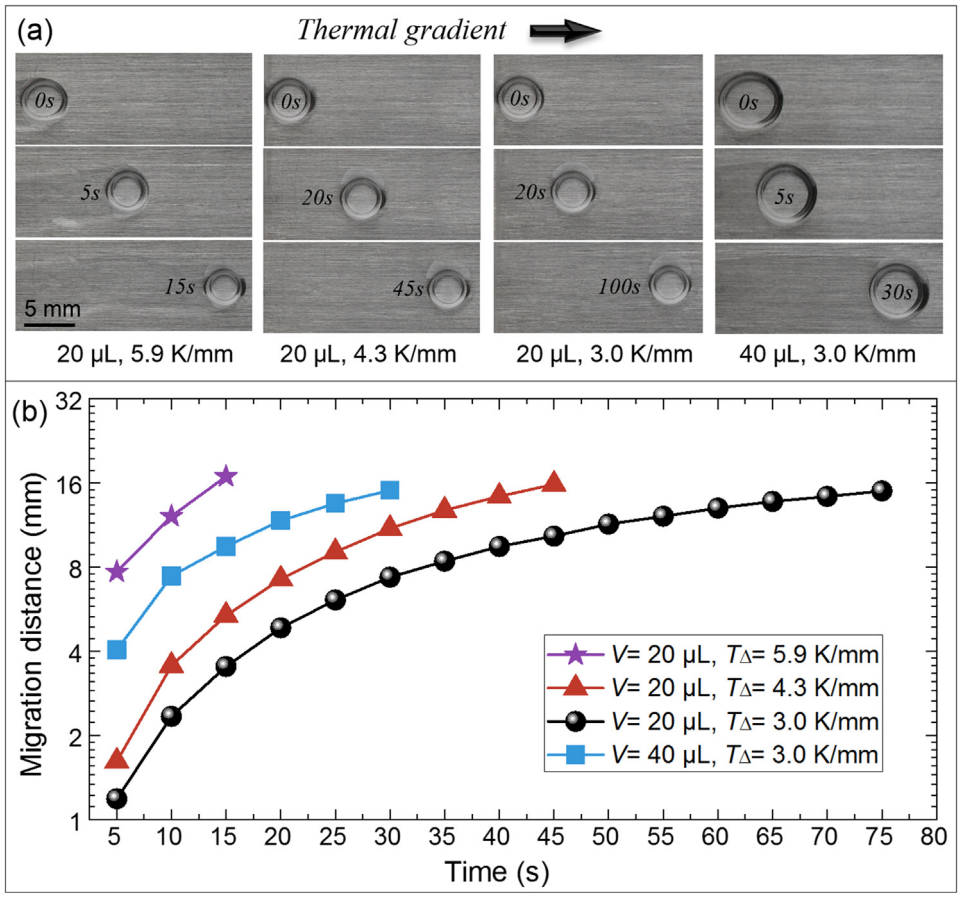

Fig. 2. Migration of silicone oil bridges with different volumes between horizontal parallel plates under different thermal gradients: (a) optical images showing the bridges at different instants in time and (b) measured migration distance versus elapsed time.

Generally, a higher thermal gradient yields a larger migration velocity, as expected. Since liquid bridges were injected between the plates at the room temperature, it takes a significant time for the liquid to thermally equilibrate with the plates. The thermal equilibration time scale can be estimated as $4h^2/k$ in which $2h$ and k denote the interface gap and thermal diffusivity, respectively. Inserting numbers one obtains a thermal equilibration time scale of 10 s.

Naturally, this estimate ignores effects due to the geometrical shape of the liquid bridge. During this time, the driving force exhibits strong variations in time. Owing to geometrical effects liquid bridges of larger volume are expected to heat up faster, which means that initially the thermocapillary driving force of larger bridges is higher. This is the probable reason why initially the 40 μL liquid bridge is faster than the 20 μL liquid bridge (at 3 K/mm). After this initial phase, however, the 20 μL liquid bridge exhibits a faster migration speed than the 40 μL liquid bridge. To further analyze this phenomenon, let us denote the diameter of a bridge's footprint at the solid surface D. A simple scaling analysis (assuming a fixed temperature derivative of surface tension and a constant temperature gradient) shows that the thermocapillary driving force scales as D, while the viscous dissipation force scales as D^2. From this we expect that liquid bridges with larger volume have a smaller migration velocity, which is what is found for the 20 μL and the 40 μL bridge (at 3 K/mm) when disregarding the first 5 s of the migration process.

Another observation that can be made in Fig. 2b is that the migration speed decreases as a function of time. This happens because the liquid viscosity increases with decreasing temperature. Since the temperature of the liquid decreases with migration distance, the viscous resistance increases.

3.2. Migration of liquid bridges between tilted parallel plates

Fig. 3a shows the influence of the tilt angle on the migration of a liquid bridge (40 μL) subject to a thermal gradient of 4.3 K/mm. Fig. 3b is a sketch showing the definition of the tilt angle. When the tilt angle is 0°, the migration speed is fastest. As the tilt angle increases, not all liquid bridges migrate as far as 16 mm, hence, the migration distance within the first 30 s is displayed for comparison, as well as the average migration velocity. Note that the migration distance decreases rapidly with increasing tilt angle, and motion is completely suspended when the tilt angle increases to 2.8°. When further increasing the tilt angle, liquid bridges would move in the opposite direction.

Then, experiments were conducted to determine the critical tilt angle at which migration is suspended. As shown in Fig. 3c, a larger critical tilt angle is needed to keep a liquid bridge suspended under a higher thermal gradient. It is interesting to see that liquid bridges with a smaller volume have a larger critical tilt angle. Under a thermal gradient of 3.0 K/mm, the critical tilt angle of a liquid bridge with a volume of 20 μL was 1.8°, which is 50% higher than that (1.2°) of a 40 μL liquid bridge. This is because the thermocapillary force is a surface force, scaling with D, while the gravitational force is a volume force, scaling with D^2. When further increasing the volume to 400 μL, liquid completely spread in the width direction of the channel. It is confirmed that a critical tilt angle also exists for these liquid bridges with a large volume, and

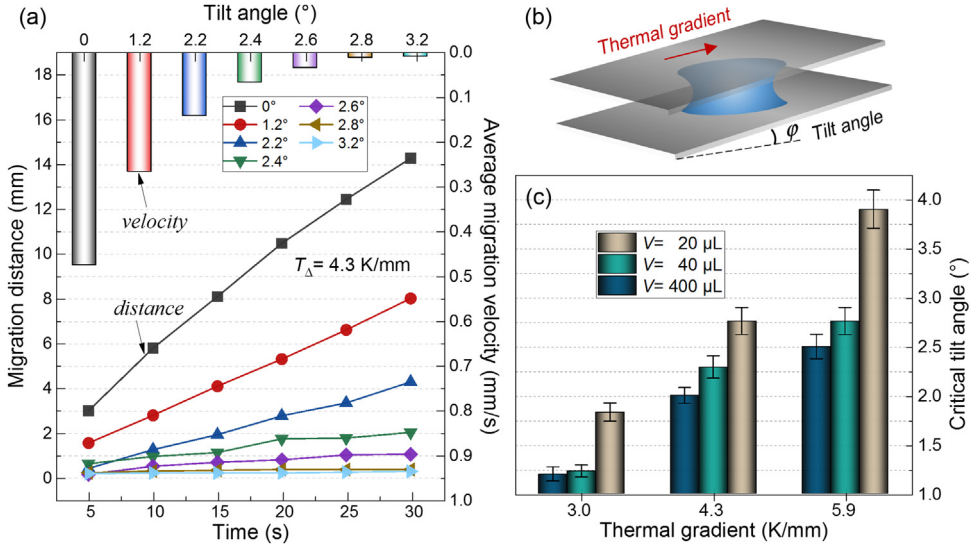

Fig. 3. (a) Effect of tilt angle on the migration of a liquid bridge (40 μL) subject to a thermal gradient of 4.3 K/mm. (b) Schematic showing the definition of the tilt angle. (c) Critical tilt angles for different thermal gradients and liquid volumes.

the values (navy blue histogram) are smaller than those of a 40 μL liquid bridge.

To rationalize these results, a theoretical model was developed (see Section 3.4). The model provides a simple framework to understand some of the key features of the thermocapillary migration of liquid bridges. The predictions of this model will be compared with the experimental data for the tilt angle.

3.3. Migration of air bubbles

Following the results presented in Fig. 3c, it is known that increasing the volume of the liquid bridge from 20 μL to 400 μL yields a corresponding decrease of the critical tilt angle. When the volume of a liquid bridge further increases to approximately 1 mL (not yet completely filling the space between the parallel plates), one can hardly observe any liquid flow even when the parallel plates are arranged horizontally. However, it was noticed that air bubbles having nucleated in the liquid lubricant migrate in the opposite direction (compared to liquid bridges), that is, from the cold to the hot end.

To confirm this result, the space between the plates was completely filled with liquid, and then an air bubble with a specific volume was injected between the surfaces via a microsyringe (diameter of needle: 0.4 mm, at room temperature) within a short period of approximately 1 s. Fig. 4b shows the migration behavior of air bubbles with different volumes of 20, 40 and 60 μL under a thermal gradient of 4.3 K/mm between horizontal parallel plates. The detailed migration process of the 40 μL air bubble can be seen in the Video S2 (in Supplementary material). The air bubbles always migrate from the cold to the hot end. To analyze the results regarding the bubble migration, we disregard the first few seconds of the migration process, as in the case of liquid bridges. It can be seen that bubbles of smaller volume migrate faster, which becomes most obvious by comparing the data for 20 µL and 60 µL bubbles.

Once an air bubble is injected into a liquid film, a surface tension gradient is generated, yielding a liquid flow from the hot region (low surface tension) to the cold region (high surface tension). This results in a motion of the bubble relative to the liquid, towards the hot side. The fundamental mechanism underlying the thermocapillary migration of air bubbles has already been reported, albeit for bubbles submerged in a pool of water under the influence of buoyancy [34–36]. Here it is demonstrated that the same mechanism also sets air bubbles sandwiched between two flat plates in motion. One thing in common between air bubbles and liquid bridges is that the thermocapillary driving force scales as D. The viscous force, however, is more difficult to analyze than in the case of liquid bridges, since viscous dissipation mainly occurs exterior to the bubble. In a recent paper, the viscous dissipation around a gas bubble rising between parallel plates was analyzed [37]. It was found that the viscous force scales as D^2. Therefore, equating the viscous force with the thermocapillary driving force results in an increasing importance of viscous dissipation as the bubble volume increases and the prediction that larger bubbles should migrate more slowly than smaller ones, in agreement with what is shown in Fig. 4b.

3.4. Mechanism of thermocapillary migration of liquid bridges

3.4.1. Theoretical model

In the following, a theoretical model is formulated to capture the key features of thermocapillary migration of liquid bridges. Before that, relevant dimensionless numbers are evaluated to check the validity of the assumptions underlying the model. For the liquid bridges investigated in this study, the mean orders of magnitudes of Reynolds number ($\frac{\rho UD}{\mu}$, $\sim 10^{-2}$) and Weber number ($\frac{\rho U^2 D}{\gamma}$, $\sim 10^{-4}$) are rather low (where ρ is the mass density, U the velocity, D the footprint of the liquid bridge, μ the dynamic viscosity, and γ the surface tension), so it is reasonable to neglect all effects related to inertia. A laminar flow field can be assumed at such low Reynolds numbers, where the viscous forces are dominant. Moreover, it is assumed that the shape of the liquid bridge is the same as in the static case without gravitation. As far as the influence of viscous stresses is concerned, this assumption is justified by the mean magnitude of the capillary number ($\frac{\mu U}{\gamma}$, $\sim 10^{-3}$). The influence of gravitation cannot be argued away that easily, since the Bond number ($\frac{\rho g D^2}{\gamma}$, ~ 10) is not small. In the model it is assumed that the liquid surfaces on both sides of the bridge are circular arcs. To check the validity of this assumption, we have compared the liquid surface shapes obtained from side-view images with circular arcs (see Fig. S2). The comparison shows that, taking into account our requirements concerning the accuracy of the model, circular arcs represent the liquid surface with reasonable accuracy.

The Young-Laplace equation describes the capillary pressure difference sustained across the interface between two fluids due to interfacial tension. As shown in Fig. 5, taking the cross sec-

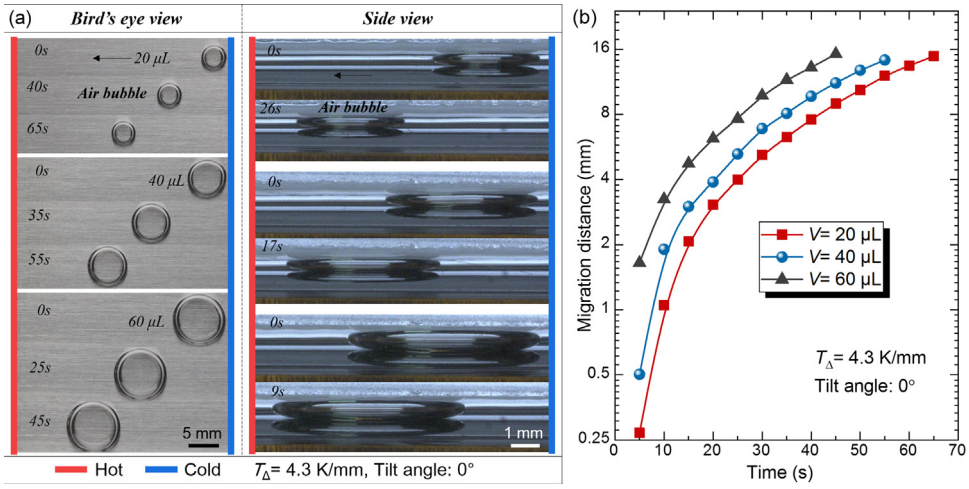

Fig. 4. Migration of air bubbles with different volumes between horizontal parallel plates completely filled with liquid under a thermal gradient of 4.3 K/mm: (a) bird's eye and side views of the migration process, and (b) measured migration distance versus elapsed time.

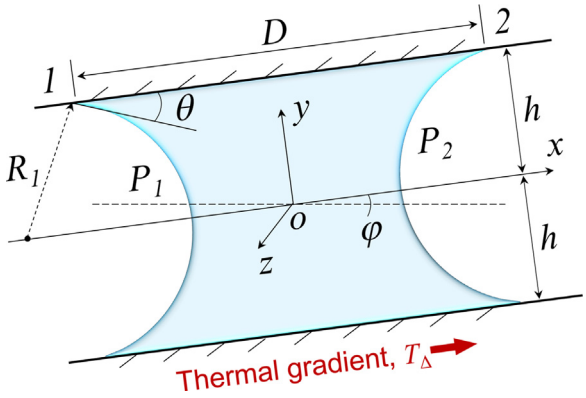

Fig. 5. Schematic of a liquid bridge between tilted parallel plates.

tion through the center of the liquid bridge as a reference, a two-dimensional model is established. It is assumed that the menisci at the left and right sides are circular arcs. The pressure drop P across the liquid surface can be written as:

$$P = \frac{\gamma}{R} = \frac{\gamma \cos\theta}{h}, \tag{1}$$

where h is half the height of the liquid bridge, and θ is the apparent contact angle.

The surface tension of liquid varies as a function of temperature, and the variation can be approximated as:

$$\gamma = \gamma_0 + \frac{\partial \gamma}{\partial x} x = \gamma_0 + T_\Delta \gamma_T x, \tag{2}$$

where γ_0 is the surface tension of the liquid at a reference temperature, γ_T is the temperature derivative of the surface tension, and T_Δ is the thermal gradient along the solid surfaces.

Notably, this model for the surface tension variation assumes that the liquid surface is thermally equilibrated with the solid surfaces, which will not be the case during the first moments after the liquid has been injected between the plates. Thus, the curved interface induced pressure difference $\Delta P_{Laplace}$ between the cold and the hot side of a liquid bridge can be written as:

$$\Delta P_{Laplace} = P_1 - P_2 = \frac{\gamma_1 \cos\theta}{h} - \frac{\gamma_2 \cos\theta}{h} = \frac{T_\Delta \gamma_T D}{h} \cos\theta, \tag{3}$$

where D is the diameter of the liquid bridge's footprint at the solid surface. Strictly, it is an approximation to use the same contact angle θ at both sides of the liquid bridge. Contact-angle hysteresis results in different contact angles at the two sides. However, in the scenario studied in this paper, there are small differences between the advancing and the receding contact angle (the measured results are provided in Fig. S3). Therefore, the apparent contact angle is used for the theoretical model.

Since the thermocapillary motion of liquid bridges is relatively slow, the corresponding flow can be regarded as laminar. With the additional simplifying assumption that end effects (close to the liquid surfaces) are negligible, only the x-component of the flow velocity needs to be considered, and the momentum equation simplifies to:

$$\frac{\partial^2 u}{\partial y^2} = \frac{1}{\mu}\frac{\partial P}{\partial x} = \frac{1}{\mu}\frac{\Delta P}{D}, \tag{4}$$

where u is the velocity component in x-direction, and$\Delta P$is the pressure difference between the cold and the hot side.

Assuming the no-slip boundary condition at the surfaces of the plates, the boundary condition in the lab frame can be written as:

$$u|_{y=\pm h} = 0 \tag{5}$$

Integrating Eq. (4) with the boundary condition (Eq. (5)), the velocity field is obtained as:

$$u = \frac{\Delta P}{2\mu D}\left(h^2 - y^2\right) \tag{6}$$

The average migration velocity of a liquid bridge is obtained as:

$$U_{Average} = \frac{1}{2h}\int_{-h}^{h} u dy = \frac{h^2}{3\mu D}\Delta P \tag{7}$$

If the parallel plates are tilted (angle of φ in Fig. 5), gravity influences the motion of a liquid bridge. The hydrostatic pressure due to the gravitational force is given by:

$$\Delta P_{gravity} = \frac{\rho V g \sin\varphi}{2hD}, \tag{8}$$

where V is the volume of the liquid bridge.

During steady-state motion of a liquid bridge, the net external pressure balances the dynamic pressure, that is:

$$\Delta P = \Delta P_{Laplace} - \Delta P_{gravity} \tag{9}$$

Substituting Eqs. (3), (8) and (9) into Eq. (7), and rearranging gives:

$$U_{Average} = \frac{h}{3\mu}\left[T_\Delta \gamma_T \cos\theta - \frac{\rho V g \sin\varphi}{2D^2}\right] \tag{10}$$

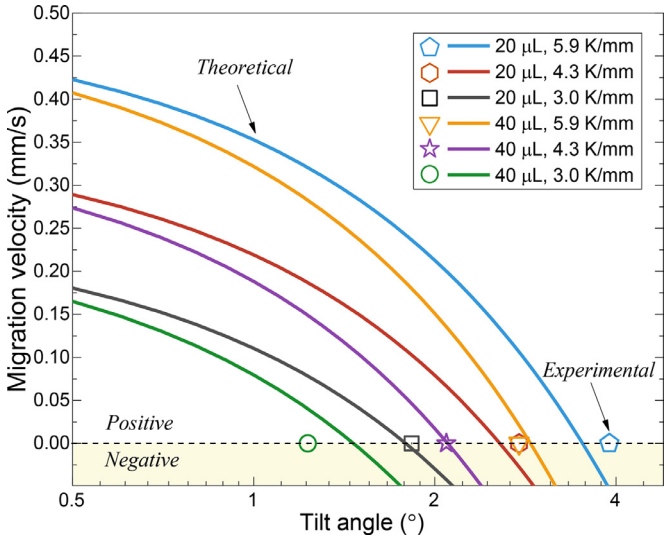

Fig. 6. Comparison between experimental (symbols) and theoretical (lines) results related to the migration of liquid bridges. The theoretical curves depict the migration velocity as a function of tilt angle, and the experimental data points indicate the critical tilt angle.

3.4.2. Validation

Fig. 6 shows a comparison between experimental (symbols) and theoretical (lines) results related to the migration of liquid bridges with volumes of 20 and 40 μL and thermal gradients of 3.0, 4.3 and 5.9 K/mm. As the line diagrams show, the theoretical migration velocity decreases with the tilt angle. As suggested by the scaling arguments presented above, a liquid bridge with a larger volume has a smaller migration velocity. The theoretical critical tilt angles are the points where the curves intersect the x-axis. It can be seen that the theoretical model approximately predicts the critical tilt angles. Given the simplicity of the model, the agreement between the theoretical and the experimental data can be considered reasonably good. Increasing the tilt angle beyond its critical value would yield a negative migration velocity, which means that liquid bridges would slide down against the thermal gradient.

Note that for the silicone oil used in this study, the variation of viscosity and surface tension with respect to the temperature can be approximated by $\mu(T) = \mu_0 e^{-0.018(T-T_0)}$ and $\gamma(T) = \gamma_0 - 0.046(T-T_0)$, respectively (where μ_0 and $\mu(T)$ represent the viscosity at the reference temperature T_0 (298 K) and T, respectively; and γ_0 and $\gamma(T)$ represent the surface tension at the reference temperature T_0 (298 K) and temperature T, respectively). Indeed, we treat the temperature dependencies of the viscosity and of the surface tension on a different footing. The reason is that without any temperature dependence of the surface tension, there would be no driving force, and the model would become meaningless. Compared to that, in the framework of the minimal model we intended to build, the temperature dependence of the viscosity is not a central aspect.

Fundamentally, it is the thermal gradient induced surface tension gradient that yields the migration of a liquid bridge from the hot to the cold side. For the liquid bridges under consideration, the ratio between the heat conduction time scale ($4h^2/k$) and the advection time scale (D/U) is approximately 1. This means that based on this simple estimate and for the set of parameters underlying our work, it is questionable if the thermal equilibration is fast enough to justify the assumption that the temperatures of the liquid surfaces at the two ends of a bridge are given by the corresponding temperatures of the plates. It needs to be taken into account, however, that the heat conduction time scale only represents an upper limit to the thermal equilibration time scale, since convective transport of heat due to the recirculation zones inside a liquid bridge reduces the thermal equilibration time scale. In any case, the comparatively long thermal equilibration time scale is the fundamental reason why we do not report the results of the model for the trajectories of liquid bridges, even if the theoretical migration velocities roughly agree with the corresponding experimental values. Still, this model is fundamentally useful, among others since the thermal equilibration time scale scales as h^2, which means that it could well be applied to compute trajectories of liquid bridges in narrower gaps.

3.5. Outlook

Overall, rational utilization of external thermal gradients can control the thermocapillary migration of liquid bridges or air bubbles between parallel plates effectively. In practical engineering applications, the leakage of liquid lubricants is widely encountered in mechanical seals operating under extreme conditions, in which liquid lubricants are depleted either due to the high pressure difference or the fast rotational speed. Taking advancing of the thermocapillary effect, one can continuously collect the lost liquid, transport it to the designated area, and eventually maintain the liquid between the two surfaces. Fig. 7 shows a preliminary design concept to manipulate the leaked liquid between parallel surfaces via an external thermal gradient. Parallel plates are constructed with an upper plate that is a quartz glass wafer and a lower plate of stainless steel 316. The interface gap is 1.25 mm and the radial thermal gradient is 5 K/mm (more detailed information about this experimental apparatus is provided in Fig. S4). When randomly injecting liquid bridges at the outer boundary, they all migrate to the center, as expected. This preliminary experiment demonstrates the feasibility of the design principle based on thermocapillary migration.

4. Conclusions

In conclusion, liquid bridges and air bubbles migrate between parallel plates when exposed to a thermal gradient. The migration velocity increases with increasing thermal gradient. When the plates are arranged horizontally, a smaller volume of bridges of bubbles yields a higher migration velocity. When tilting the plates, the thermocapillary migration of liquid bridges is suspended when

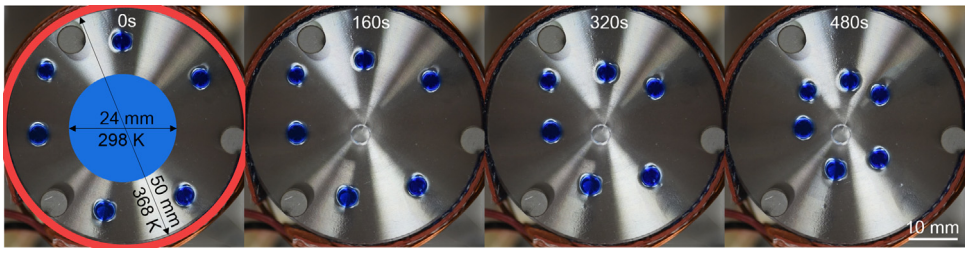

Fig. 7. Manipulating liquid bridges between parallel surfaces via an external thermal gradient.

a critical tilt angle is reached. The critical tilt angle decreases with increasing liquid volume. An explanation for these observations was provided based on scaling relationships for the thermocapillary force, the gravity-induced force and the viscous force. A simple two-dimensional theoretical model was developed that describes the thermocapillary migration of liquid bridges. The model is able to predict the critical tilt angles with decent accuracy. Based on the observed effects, a design principle for the replenishment of liquid in tribological systems is proposed.

Declaration of Competing Interest

The authors declare that they have no known competing financial interests or personal relationships that could have appeared to influence the work reported in this paper.

CRediT authorship contribution statement

Qingwen Dai: Writing – original draft, Writing – review & editing. **Sangqiu Chen:** Formal analysis, Investigation. **Wei Huang:** Visualization, Investigation. **Xiaolei Wang:** Supervision, Resources. **Steffen Hardt:** Writing – review & editing, Writing – original draft.

Acknowledgments

The authors are grateful for the support provided by Alexander von Humboldt-Stiftung, National Natural Science Foundation of China (Grant No. 51805252), and the Aeronautical Science Foundation of China (No. 2020Z040052002).

Supplementary materials

Supplementary material associated with this article can be found, in the online version, at doi:10.1016/j.ijheatmasstransfer.2021.121962.

References

[1] D.T. Wasan, A.D. Nikolov, H. Brenner, Droplets speeding on surfaces, Science 291 (5504) (2001) 605–606.
[2] X.F. Xu, J.B. Luo, Marangoni flow in an evaporating water droplet, Appl. Phys. Lett. 91 (12) (2007) 124102.
[3] R. Tadmor, Marangoni flow revisited, J. Colloid Interface Sci. 332 (2) (2009) 451–454.
[4] T. Baier, C. Steffes, S. Hardt, Thermocapillary flow on superhydrophobic surfaces, Phys. Rev. E Stat. Nonlinear Soft Matter Phys. 82 (3 Pt 2) (2010) 037301.
[5] N. Bjelobrk, H.-.L. Girard, S. Bengaluru Subramanyam, H.-.M. Kwon, D. Quéré, K.K. Varanasi, Thermocapillary motion on lubricant-impregnated surfaces, Phys. Rev. Fluids 1 (6) (2016) 063902.
[6] C. Lv, S.N. Varanakkottu, T. Baier, S. Hardt, Controlling the trajectories of nano/micro particles using light-actuated marangoni flow, Nano Lett. 18 (11) (2018) 6924–6930.
[7] C. Bakli, P.D.S. Hari, S. Chakraborty, Mimicking wettability alterations using temperature gradients for water nanodroplets, Nanoscale 9 (34) (2017) 12509–12515.
[8] C. Li, D. Zhao, J. Wen, X. Lu, Numerical investigation of wafer drying induced by the thermal marangoni effect, Int. J. Heat Mass Tran. 132 (2019) 689–698.
[9] Q.W. Dai, M.M. Khonsari, C. Shen, W. Huang, X.L. Wang, Thermocapillary migration of liquid droplets induced by a unidirectional thermal gradient, Langmuir 32 (30) (2016) 7485–7492.
[10] P.G. Grützmacher, A. Rosenkranz, A. Szurdak, C. Gachot, G. Hirt, F. Mücklich, Lubricant migration on stainless steel induced by bio-inspired multi-scale surface patterns, Mater Design 150 (2018) 55–63.
[11] G. Karapetsas, K.C. Sahu, K. Sefiane, O.K. Matar, Thermocapillary-driven motion of a sessile drop: effect of non-monotonic dependence of surface tension on temperature, Langmuir 30 (15) (2014) 4310–4321.
[12] D. Mamalis, V. Koutsos, K. Sefiane, On the motion of a sessile drop on an incline: effect of non-monotonic thermocapillary stresses, Appl. Phys. Lett. 109 (23) (2016) 231601.
[13] H. Liu, L. Wu, Y. Ba, G. Xi, A lattice boltzmann method for axisymmetric thermocapillary flows, Int. J. Heat Mass Tran 104 (2017) 337–350.
[14] R. Wang, S. Bai, Modeling and experimental analysis of thermocapillary effect on laser grooved surfaces at high temperature, Appl. Surf Sci. 465 (2019) 41–47.
[15] C. Liu, I. Legchenkova, L. Han, W. Ge, C. Lv, S. Feng, E. Bormashenko, Y. Liu, Directional droplet transport mediated by circular groove arrays. Part i: experimental findings, Langmuir 36 (32) (2020) 9608–9615.
[16] Q.W. Dai, W. Huang, X.L. Wang, M.M. Khonsari, Directional interfacial motion of liquids: fundamentals, evaluations, and manipulation strategies, Tribol. Int. 154 (2021) 106749.
[17] H.P. Greenspan, On the motion of a small viscous droplet that wets a surface, J. Fluid Mech. 84 (1978) 125–143.
[18] F. Brochard, Motions of droplets on solid surfaces induced by chemical or thermal gradients, Langmuir 5 (2) (1989) 432–438.
[19] M.L. Ford, A. Nadim, Thermocapillary migration of an attached drop on a solid surface, Phys. Fluids 6 (9) (1994) 3183–3185.
[20] V. Pratap, N. Moumen, R.S. Subramanian, Thermocapillary motion of a liquid drop on a horizontal solid surface, Langmuir 24 (9) (2008) 5185–5193.
[21] Q.W. Dai, W. Huang, X.L. Wang, M.M. Khonsari, Ringlike migration of a droplet propelled by an omnidirectional thermal gradient, Langmuir 34 (13) (2018) 3806–3812.
[22] M. Foroutan, S.M. Fatemi, F. Esmaeilian, V.F. Naeini, M. Baniassadi, Contact angle hysteresis and motion behaviors of a water nano-droplet on suspended graphene under temperature gradient, Phys. Fluids 30 (5) (2018) 052101.
[23] D.M. Anderson, S.H. Davis, The spreading of volatile liquid droplets on heated surfaces, Phys. Fluids 7 (2) (1995) 248.
[24] C.J. Lv, C. Chen, Y.C. Chuang, F.G. Tseng, Y.J. Yin, F. Grey, Q.S. Zheng, Substrate curvature gradient drives rapid droplet motion, Phys. Rev. Lett. 113 (2) (2014) 5.
[25] P.F. Zhang, H.W. Chen, L. Li, H.L. Liu, G. Liu, L.W. Zhang, D.Y. Zhang, L. Jiang, Bioinspired smart peristome surface for temperature-controlled unidirectional water spreading, Acs Appl. Mater Inter 9 (6) (2017) 5645–5652.
[26] E. Bormashenko, Wetting of flat gradient surfaces, J. Colloid Interface Sci. 515 (2018) 264–267.
[27] Y. Kita, C.M. Dover, A. Askounis, Y. Takata, K. Sefiane, Drop mobility on superhydrophobic microstructured surfaces with wettability contrasts, Soft Matter 14 (46) (2018) 9418–9424.
[28] Q.W. Dai, Z.D. Hu, W. Huang, X.L. Wang, Controlled support of a magnetic fluid at a superhydrophobic interface, Appl. Phys. Lett. 116 (22) (2020) 221601.
[29] J. Li, X.L. Tian, A.P. Perros, S. Franssila, V. Jokinen, Self-propelling and positioning of droplets using continuous topography gradient surface, Adv. Mater Inter. 1 (3) (2014) 1400001.
[30] D. Liu, K. Li, S. Zhang, T. Amann, C. Zhang, X. Yan, Anti-spreading behavior of 1,3-diketone lubricating oil on steel surfaces, Tribol. Int. 121 (2018) 108–113.
[31] N. Sinn, M.T. Schür, S. Hardt, No-contact electrostatic manipulation of droplets on liquid-infused surfaces: experiments and numerical simulations, Appl. Phys. Lett. 114 (21) (2019) 213704.
[32] L. Qi, Y. Niu, C. Ruck, Y. Zhao, Mechanical-activated digital microfluidics with gradient surface wettability, Lab Chip 19 (2) (2019) 223–232.
[33] Q.W. Dai, Z.J. Chong, W. Huang, X.L. Wang, Migration of liquid bridges at the interface of spheres and plates with an imposed thermal gradient, Langmuir 36 (22) (2020) 6268–6276.
[34] N.O. Young, J.S. Goldstein, M.J. Block, The motion of bubbles in a vertical temperature gradient, J. Fluid Mech. 6 (3) (1959) 350–356.
[35] S. Nas, G. Tryggvason, Thermocapillary interaction of two bubbles or drops, Int. J. Multiphase Flow 29 (7) (2003) 1117–1135.
[36] Y. Alhendal, A. Turan, Thermocapillary bubble dynamics in a 2d axis swirl domain, Heat Mass Transf. 51 (4) (2014) 529–542.
[37] M. Murano, K. Okumura, Rising bubble in a cell with a high aspect ratio cross–section filled with a viscous fluid and its connection to viscous fingering, Phys. Rev. Res. 2 (1) (2020) 013188.